Superior Sensing Properties of Black Phosphorus as Gas Sensors: A Case Study on the Volatile Organic Compounds

*Pengfei Ou, Pengfei Song, Xinyu Liu, and Jun Song**

The unique structure and prominent properties of black phosphorus (BP) and its monolayer and multilayers in device applications have attracted significant attention to this elemental 2D material. In this study, a comprehensive evaluation of the candidacy of monolayer BP as a channel material for high-performance volatile organic compound (VOC) sensors is conducted combining first-principles density functional theory calculations and non-equilibrium Green's function formalism. The adsorption configurations and energetics of several typical VOCs (ethanol, propionaldehyde, acetone, toluene, and hexane) on monolayer BP are examined and it is demonstrated that VOCs generally exhibit stronger interaction with monolayer BP than with the widely studied monolayer MoS_2, indicative of monolayer BP potentially being a more sensitive VOC sensor. Monolayer BP is shown to exhibit highly anisotropic transport behaviors, whereas the absolute modification of current–voltage responses due to VOCs is found to show a trend that is direction independent. Moreover, the adsorption of VOCs on monolayer BP is strong enough to resist thermal disturbance, yet allows fast recovery time. The results suggest that BP is a compelling and feasible candidate for sensing applications of VOCs.

1. Introduction

Since the discovery of the wonder material graphene,[1] new 2D materials with novel electronic and optoelectronic properties continue to emerge. The 2D counterpart of black phosphorus (BP), being the most stable form among numerous allotropes of elemental phosphorus and introduced as "phosphorene,"[2] has received great attention recently due to its great promise for use in optoelectronic devices,[3–6] memory devices,[7,8] radio frequency transistors,[9] Schottky diodes,[10–13] and energy storage/conversion systems.[14,15] BP has a layered structure and the interaction in few-layer BP is associated with a significant charge redistribution, caused by the non-local electron–electron correlations.[16] Within the monolayer BP that comprises puckered honeycomb structure, each phosphorus atom is bonded covalently with three adjacent phosphorus atoms, arranged in a non-planar fashion.[17–20] Atomically thin BP flakes have been successfully fabricated by methods of micromechanical cleavage using an adhesive tape from their parent bulk crystal,[17,21] liquid-phase exfoliation,[22,23] and plasma-assisted fabrication.[24] Besides, the band gap of monolayer BP is measured to be ≈1.45 eV by photoluminescence spectra.[2]

Among various applications of monolayer and/or multilayer BP, one promising area is its usage in gas/molecule sensors for environmental analysis or bioanalysis. Numerical theoretical studies have been performed to investigate the sensing properties of BP.[25,26] Kou et al.[25] studied the adsorption properties of CO, CO_2, NH_3, NO, and NO_2 on monolayer BP using first-principles calculations. They demonstrated that those gas molecules, when adsorbed on monolayer, act as donors or acceptors and cause the modification of electronic properties. A larger change in, for example, the band structure and/or charge transfer, indicates a high sensitivity. Their results show that monolayer BP is more sensitive to NO and NO_2, indicating possible application of monolayer BP to nitrogen-based gas induction. Moreover, Kou et al.[25] showed that different gas molecules lead to distinctive current–voltage (I–V) responses, for example, the adsorption of NH_3 or NO induces reduction and increase of current, respectively. In another study, Suvansinpan et al.[26] performed first-principles calculations to study metal-doped monolayer BP. For the group of metal dopants (i.e., alkali [Li and Na], p-shell [Al, Pb, and Bi], 3d [Fe, Co, and Ni], 4d [Pd and Ag], and 5d [Au and Pt]) examined, it was shown that metal doping generally enhances the chemical activity of monolayer BP in sensing NO molecules.

On the experimental side, Abbas et al.[27] reported the pioneer study on the chemical sensibility of NO_2 by field-effect transistors (FETs) based on multilayer BP. They showed that the BP sensors exhibit enhanced conduction and high sensitivity when exposed to NO_2 down to 5 ppb, and further when the multilayer BP is

P. Ou, Prof. J. Song
Department of Mining and Materials Engineering
McGill University
Montreal, QC, H3A 0C5, Canada
E-mail: jun.song2@mcgill.ca
Dr. P. Song
Department of Mechanical Engineering
McGill University
Montreal, QC, H3A 0C3, Canada
Dr. P. Song, Prof. X. Liu
Department of Mechanical and Industrial Engineering
University of Toronto
Toronto, ON, M5S 3G8, Canada

The ORCID identification number(s) for the author(s) of this article can be found under https://doi.org/10.1002/adts.201800103

DOI: 10.1002/adts.201800103

exposed to NO_2 concentrations of 5, 10, 20, and 40 ppb, the relative conduction changes in FETs followed the Langmuir isotherm for molecules adsorbed on the surface. The systematic enhancement in conductance with the increase in NO_2 concentration indicated that BP was doped with holes and the NO_2 molecules withdraw electrons from BP. It was confirmed that the charge transfer between BP and NO_2 is the dominant sensing mechanism. Compared with other 2D materials, such as MoS_2,[28,29] the sensitivity of multilayer BP was found to be significantly higher.[27] For instance, the conductance change in a 55 nm multilayer BP exposed to 5 ppb NO_2 was 2.9%, whereas the relative change for an 18 nm thick MoS_2 to 1200 ppb NO_2 was only approximately 1.0%. Cui et al.[30] investigated NO_2 sensing properties of multilayer BP as its thickness varies and proposed that a thickness of 4.8 nm led to the maximum response of the devices. Recently, Cho et al.[31] accurately compared various aspects of the NO_2 sensing performance (i.e., adsorption behavior, selectivity, response/recovery time, and mole response factor) of chemically exfoliated BP, MoS_2, and graphene with similar flake-size distribution (on average ≈400 nm). The electrical sensing measurements showed that the sensitivity (molar response factor) and response of BP can be up to 20 times higher and 40 times faster than those of MoS_2 and graphene when working at 0.1–100 ppm levels.

In addition to NO_2 detection, multilayer BP has also been shown to be a promising material for methanol and hydrogen sensors. Mayorga-Martinez et al.[32] demonstrated that BP is capable of detecting methanol vapor with electrochemical impedance spectroscopy. The impedance phase that measured at a constant frequency is used for selective quantification of methanol. The low detection limit (LOD) of 28 ppm in this BP vapor sensor is substantially below the approved exposure limit of 200 ppm. This vapor sensing system displayed a high selectivity to methanol at a constant frequency of 1 kHz, a good stability over a 20-day period, as well as a long-term response of about 90% of its initial response for 1140 ppm methanol vapor. Lee et al.[33] recently functionalized exfoliated multilayer BP flakes with Pt nanoparticles and showed that a significant electrical response to H_2 can be achieved by the Pt-functionalized BP sensors with a drain–source current decreased from 2.46 to 1.17 μA under the voltage of +10 meV. They also showed that when the sensor was exposed to a low concentration (4%) H_2 gas, the I_{ON}/I_{OFF} and μ_{eff} ratio increased by 115% and 15.6%. Sensing of H_2 by BP-based sensors has also been studied by Cho et al.,[34] which showed that noble metal (i.e., Au and Pt) incorporated BP enables detection of low concentration of H_2 with high response amplitude. In particular, the as-synthesized Pt/BP sensor exhibited selective response and is highly sensitive to approximately 1% concentration H_2 gas with a resistance variation of ≈500% in the channel, showing that heteroatom doping process is an effective way to modify the intrinsic properties and tune the H_2 sensing properties of BP. However, the mechanism underlying this Pt-incorporation induced highly selective H_2 gas sensing is still need to be clarified.

In the present study, we will limit our discussion of BP in its application to the sensing of volatile organic compounds (VOCs) as a case study. VOCs are defined as organic compounds with relatively high volatility or vapor pressure, many of which can be highly neurotoxic and/or cause long-term compounding health concerns. The analysis of VOCs in exhaled air is a newly developed methodology for early-stage screening and diagnosing diseases, which is significant for enabling effective treatment and improving the survival rates of patients.[35,36] Various methods have been developed to detect the existence of VOCs, which includes gas chromatography–mass spectrometry,[37] flow-tube mass spectrometry,[38] surface acoustic wave sensors,[39] quartz crystal microbalance,[40] and chemiresistors.[36] Among various methods, the chemiresistor is particularly interesting due to its power-efficiency, cost-effectiveness, rapidness, reversibility, and high sensitivity. The detection of target VOCs in a chemiresistor is dependent on the change in electrical resistance of channel material when it interacts with analytes. Therefore, developing a highly efficient channel material is essential to the realization of a high-performance chemiresistor. Monolayer BP is considered as a promising candidate of channel for field-effect transistors due to its extraordinary properties. It has been shown to exhibit higher molecular adsorption energies than other 2D nanomaterials (such as MoS_2 and graphene),[25,31] and it possesses larger inherent surface-to-volume ratio due to its puckered lattice configuration.[41] Monolayer BP also shows less out-of-plane electrical conductance compared to other 2D nanomaterials, therefore is able to induce a much more sensitive response to target analytes near the phosphorus surface.[27] Additionally, Kou et al.[25] demonstrated that BP is a superior material for gas sensors due to its adsorption sensitive surface and distinctive *I–V* characteristics along armchair and zigzag directions. Given the extraordinary electronic properties of monolayer BP, it is highly desirable to explore and establish the trends and rules of VOCs adsorption on monolayer BP and distinguish the characteristics of the molecular influences on the transport behaviors, which can be used as effective biomarkers for diagnosing lung cancer.

In this regard, we provide the first theoretical study on the investigation of chemical sensing properties of monolayer BP with five different VOC analytes, specifically, ethanol (C_2H_5OH), propionaldehyde (C_2H_5CHO), acetone ($(CH_3)_2CO$), toluene ($C_6H_5CH_3$), and hexane (C_6H_{14}). These VOCs selected herein are representative examples which individually belongs to the VOC categories of alcohols, aldehydes, ketones, aromatic compounds, and hydrocarbons that could be the potential biomarkers for diagnosing lung cancer.[36] Employing first-principles density functional theory (DFT) calculations, preferential adsorption sites of VOCs on monolayer BP are identified and the corresponding adsorption energies are obtained. Our results demonstrate that VOCs generally exhibit stronger interaction with monolayer BP than that with the widely studied monolayer MoS_2, indicative of monolayer BP potentially being a more sensitive VOC sensor. The adsorption energetics of VOCs on monolayer BP are shown to be tunable via strain engineering. The *I–V* characteristics of monolayer BP with and without VOC adsorption are calculated using the non-equilibrium Green's function (NEGF) formalism, demonstrating highly anisotropic transport behaviors, yet the absolute modification of *I–V* responses due to VOCs is found to show a trend that is direction independent. Moreover, the simulated recovery time is well within the detectable range for most of the VOCs molecules, which indicates good reusability. Our findings suggest that monolayer can be a compelling candidate material, combining high sensitivity and fast recovery time for VOC sensors.

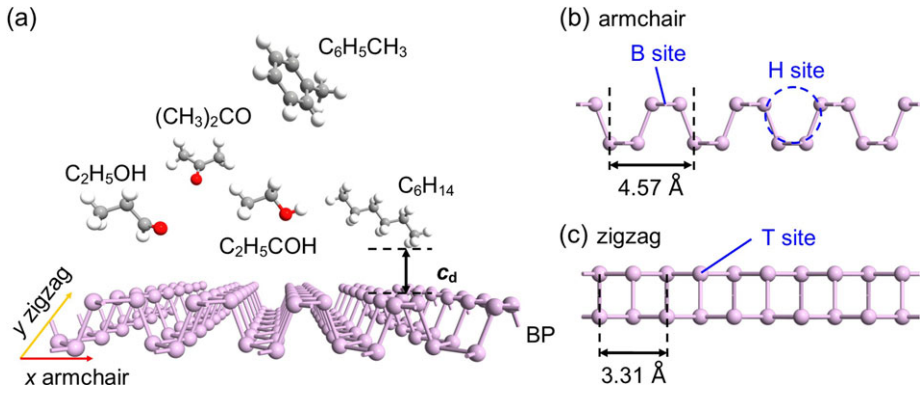

Figure 1. a) Illustrations of typical VOCs adsorbed on the monolayer BP. Side projection views along the two featured directions: b) armchair and c) zigzag directions of the atomic structure of monolayer BP, with the three types of potential sites for VOC adsorption, namely, the B-site on top of a P–P bond, H-site above the center of a hexagon, and T-site on top of a P atom indicated.

2. Methodology

2.1. First-Principles DFT Calculations

First-principles DFT calculations were employed for relaxing the structures of VOC/BP systems and computing the energetics and electronic properties. The calculations were performed using the Vienna Ab-Initio Simulation Package (VASP)[42] with exchange–correlation interaction treated in the generalized gradient approximation (Perdew–Burke–Ernzerhof functional).[43] The long-range van der Waals interactions were considered and modeled by the DFT-D2 method of Grimme.[44] A cut-off energy of 500 eV was used for the plane wave basis set, and the gamma-only and $4 \times 4 \times 1$ k-meshes were employed for the self-consistent relaxation and non-self-consistent calculations, respectively. In the calculations, the system comprises a 5×7 supercell of monolayer BP with one VOC adsorbed. Additional scaling studies were performed to confirm that this system size is sufficient to eliminate the intermolecular interaction. The in-plane lattice parameters of the monolayer BP were optimized to be $a = 4.57$ Å and $b = 3.31$ Å along armchair and zigzag directions, respectively (**Figure 1**), which are in great agreement with the values reported in previous studies.[45,46] A vacuum slab of 20 Å in thickness was added in the out-of-plane direction to eliminate interactions between periodic images. The structural relaxation was regarded as a convergence when the magnitude of the Hellmann–Feynman force fell below 0.01 eV $Å^{-1}$ for all atoms, and the energy convergence criterion for the electronic wave function was set to be 10^{-6} eV.

To identify the possible configurations for VOCs adsorption on the monolayer BP, three potential adsorption locations (Figure 1), that is, on top of i) a P–P bond (B-site), ii) the center of a hexagon (H-site), and iii) a P atom (T-site), were considered.[47] As a VOC molecule was introduced, its center of mass was positioned at one of these sites and different orientations of the molecule were evaluated. For instance, for $(CH_3)_2CO$, the molecular axis can be oriented parallel or perpendicular to the monolayer BP with either the C or O atom pointing toward the monolayer BP. The adsorption strength of a VOC on the monolayer BP can be quantitatively assessed via the adsorption energy E_{ad}, defined as

$$E_{ad} = E(\text{VOC/BP}) - E(\text{VOC}) - E(\text{BP}) \quad (1)$$

where E(VOC/BP) represents the total energy of the monolayer BP with an adsorbed VOC, while E(VOC) and E(BP), respectively, denote the energies of the corresponding isolated VOC and pristine monolayer BP. A negative value of E_{ad} indicates that the adsorption is exothermic. Furthermore, to examine the effect of strain on the VOC adsorption on the monolayer BP, biaxial strains within the lateral plane varying from −5% to 5% with an interval of 1% were applied. The strain was applied through scaling the in-plane lattice parameters of monolayer BP, for which the details can be found in our previous studies.[48,49]

2.2. Transport Property Calculations

In order to further quantitatively assess the potential of monolayer BP as a VOC sensor, the transport properties of monolayer BP prior to and post VOC adsorption were carried out using the NEGF technique within the Keldysh formalism as implemented in TranSIESTA package.[50] Geometry optimization has been achieved when the maximum difference between the output and input on each element of the Density Matrix is less than 10^{-4}. The energy cut-off for the real-space mesh was set to 150 Ry. The electron wave function was expanded using a double-ζ polarized (DZP) basis set. Monkhorst–Pack k-point grids of $1 \times 2 \times 50$ and $1 \times 2 \times 1$ were employed for electrodes and transport calculations, respectively. The current through the atomic scale system is calculated from the Landauer–Büttiker formula.[51]

$$I(V_b) = G_0 \int_{\mu_L}^{\mu_R} T(E, V_b)[f(E-\mu_L) - f(E-\mu_R)]\mathrm{d}E \quad (2)$$

where V_b is the bias voltage, μ_L and μ_R are the two electrochemical potentials of left and right leads, respectively. $T(E, V_b)$ is the transmission coefficient at energy E and bias voltage V_b, $f(E)$ is the Fermi–Dirac distribution function, and $G_0 = 2e^2/h$ is the quantum conductance. As seen from the above equation, the current is the integral of the transmission coefficient over the bias window.

Table 1. Values of the adsorption energy (E_{ad}, in meV; bold numbers indicate energetically preferable sites) and distance (c_d, in Å) of the closest atom in VOCs above the monolayer BP for VOCs adsorbed at different adsorption sites, and the charge transfers ($\Delta\rho$, in electron) from monolayer BP to the VOCs on energetically preferable site. The calculated adsorption energies of VOCs on bilayer BP, along with available adsorption energies of VOCs on monolayer MoS_2 in the literature, are also included for comparison.

	B-site		H-site		T-site		Bilayer BP		MoS_2[54]	MoS_2[54]
	E_{ad}	c_d	E_{ad}	c_d	E_{ad}	c_d	E_{ad}	$\Delta\rho$	E_{ad}[a)]	E_{ad}[b)]
C_2H_5OH	**−244**	**2.80**	−239	2.94	−241	2.86	−256	0.01	−210	−220
C_2H_5CHO	−214	2.59	**−350**	**2.44**	−211	2.60	−362	0.05	−210	−220
$(CH_3)_2CO$	−320	2.76	−247	2.77	**−328**	**2.56**	−338	0.04	−140	−160
$C_6H_5CH_3$	−432	2.47	−417	2.53	**−499**	**2.42**	−508	0.04		
C_6H_{14}	−360	2.58	−341	2.69	**−370**	**2.53**	−383	0.02		

[a)] DFT-D3 calculations; [b)] vdW-DF2 calculations.

3. Results and Discussion

For the five VOCs considered, the adsorption sites along with the associated adsorption energies and the equilibrium positions (i.e., distances) of the molecule above the monolayer BP are given in **Table 1**. The O-based VOCs generally exhibit smaller adsorption energies than hydrocarbon molecules lacking oxygen groups, namely, $C_6H_5CH_3$ and C_6H_{14}, due to fewer total number of atoms in the oxygen-functionalized VOCs. The energetically preferable adsorption configurations for different VOCs are noted in Table 1, C_2H_5OH and C_2H_5CHO prefer adsorption at the B-site and H-site with adsorption energies of −244 and −350 meV, whereas $(CH_3)_2CO$, $C_6H_5CH_3$, and C_6H_{14} prefer T-sites with adsorption energies of −328, −499, and −370 meV, respectively. It is worth noting that for all the VOCs considered, the adsorption energy is sufficiently larger to resist thermal disturbance at room temperature, that is, the magnitude of E_{ad} being much beyond k_BT (k_B is the Boltzmann constant).[52,53] As noted from Table 1, the distance of a VOC molecule from monolayer BP ranges from 2.42 to 2.94 Å, similar to those for VOC adsorption on monolayer MoS_2 previously reported by Tian et al.[54] It is also interesting to see that the most energetically preferable adsorption configuration is the site where VOC is at the shortest distance from monolayer BP, suggesting that the distance be a direct indication of the interaction strength between a VOC and a monolayer BP.

Fundamentally, the sensitivity of a channel material is dictated by the intercorrelated quantities of adsorption density or coverage, and interaction strength between the analyte and channel material, that is, the adsorption energy.[55] Larger adsorption energy would lead to more VOC molecule adsorption on the channel material and consequently enhanced sensitivity. In a previous study, Kim et al.[56] demonstrated that MoS_2 sensors exhibit high sensitivity to VOCs, specifically, down to a concentration of 1 ppm for C_2H_5CHO and $(CH_3)_2CO$ and about 10 ppm for C_2H_5OH, $C_6H_5CH_3$, and C_6H_{14}. As seen in Table 1, adsorption of VOCs on monolayer BP shows notably larger adsorption energies than those on MoS_2 (from either DFT-D3 or vdW-DF2 calculations).[54] This indicates stronger analyte–channel interaction and suggests that monolayer BP potentially may exhibit higher sensitivity to VOCs than MoS_2.

In addition, monolayer BP was theoretically predicted to hold up almost 30% critical strain,[57] signaling the potential of tuning its chemical and physical properties by strain engineering.[58] Therefore, we examine the influence of strain on the adsorption energetics of VOCs on monolayer BP. The effect of strain is demonstrated in **Figure 2** in the presentative cases of C_2H_5CHO and $C_6H_5CH_3$ adsorption. We note that the application of ±5% biaxial strain can tune the adsorption energies of C_2H_5CHO and $C_6H_5CH_3$ in the ranges of [−385, −332] and [−467, −551] meV, with compressive strain enhancing the (magnitude of) adsorption energy while tensile strain doing the opposite. The results imply that compression may be used as a means to magnify the sensibility of monolayer BP, for example, for weakly binding VOC molecules, while tension can help facilitate the removal of VOCs. Moreover, it is important to mention that those adsorption characteristics reported above are well retained as BP goes from monolayer to bilayer or even few layers, except for the fact that the adsorption energy is further enhanced, as demonstrated in Table 1, indicative of robust performance in spite of possible BP thickness variation.

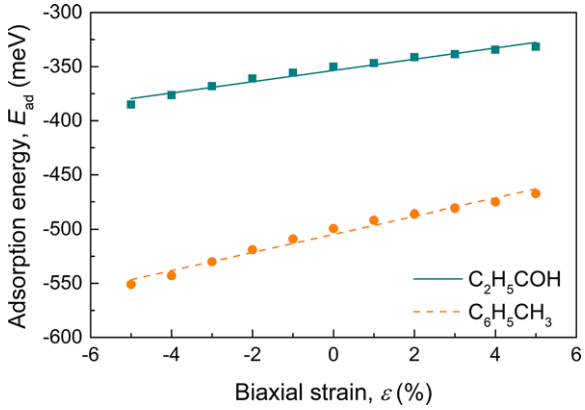

Figure 2. The adsorption energy under the application of biaxial strain for C_2H_5CHO and $C_6H_5CH_3$ adsorbed on the monolayer BP. The solid and dashed lines are fitted lines to guide the eyes.

To further elucidate the role of charge transfer between VOCs molecules and monolayer BP, we provide the isosurface plot of charge density difference for these systems. In particular, we employed the Bader charge analysis[59–62] to examine the charge density difference and thus to determine

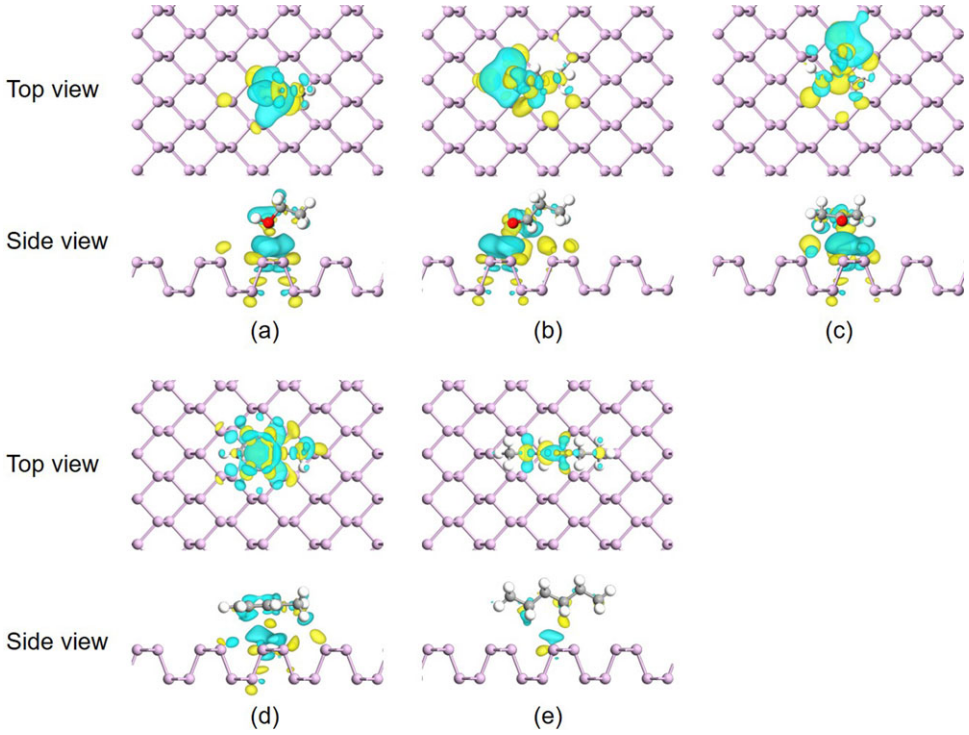

Figure 3. Top and side views of the charge density difference contour plots for a) C_2H_5OH, b) C_2H_5CHO, c) $(CH_3)_2CO$, d) $C_6H_5CH_3$, and e) C_6H_{14} adsorbed on monolayer BP (only a 4 × 4 supercell is shown for readability). The white, brown, red, and purple spheres represent hydrogen, carbon, oxygen, and phosphorus atoms, respectively. Yellow and blue colors correspond to charge accumulation and depletion, respectively. For the contour plots, the isosurface value is 0.002 e $Å^{-3}$.

the charge transfer value and direction. The charge density difference

$$\Delta\rho(r) = \rho_{VOC/BP}(r) - \rho_{VOC}(r) - \rho_{BP}(r) \quad (3)$$

is calculated from the spatial charge density distributions of the combined system ($\rho_{VOC/BP}$), isolated VOC (ρ_{VOC}), and monolayer BP (ρ_{BP}). **Figure 3** shows the charge density differences for the favorable geometries, where the charge densities of pristine monolayer BP and the isolated VOCs are separately calculated. We find that the VOCs act as charge acceptors, taking charge between 0.01 and 0.05 electrons from monolayer BP. Strong charge redistribution is observed for the cases of C_2H_5OH, C_2H_5CHO, and $(CH_3)_2CO$, as seen in Figure 3a–c, which can be attributed to the strong electronegativity of oxygen atom in those VOC molecules. On the other hand, there is significantly less charge redistribution for $C_6H_5CH_3$ and C_6H_{14} (see Figure 3d,e). Comparing the charge transfer and redistribution behaviors with those of VOCs on monolayer MoS_2,[54] C_2H_5OH acts as charge acceptor while C_2H_5CHO and $(CH_3)_2CO$ act as charge donors, when adsorbed on MoS_2. Furthermore, there is generally larger degree of charge transfer and redistribution for VOCs on monolayer BP than on monolayer MoS_2, consistent with the higher adsorption energy level.[54]

To clarify the effects of VOCs adsorption on the electronic structures, the total density of states (DOS) of monolayer BP post VOC adsorption and projected DOS from various VOCs are calculated and presented in **Figure 4**. Our calculations show that

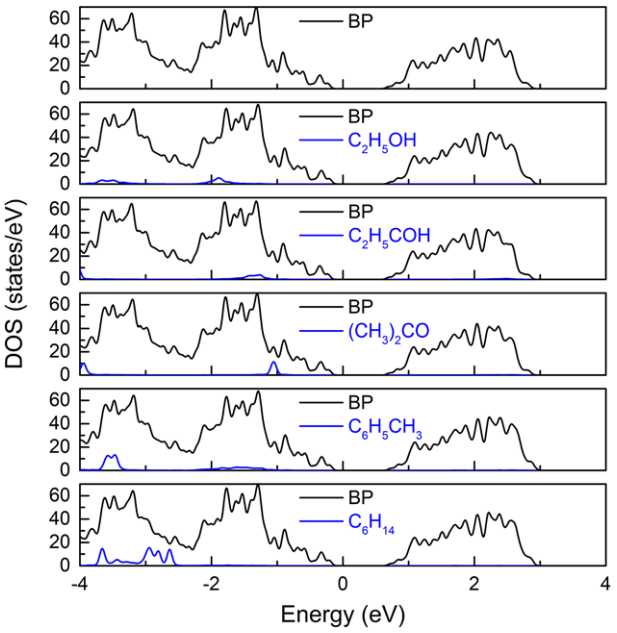

Figure 4. Density of states (DOS) plot of pristine monolayer BP (top) in comparison with the projected DOSs of monolayer BP (black) and the VOCs (blue) post adsorption. The zero-energy point corresponds to the Fermi energy.

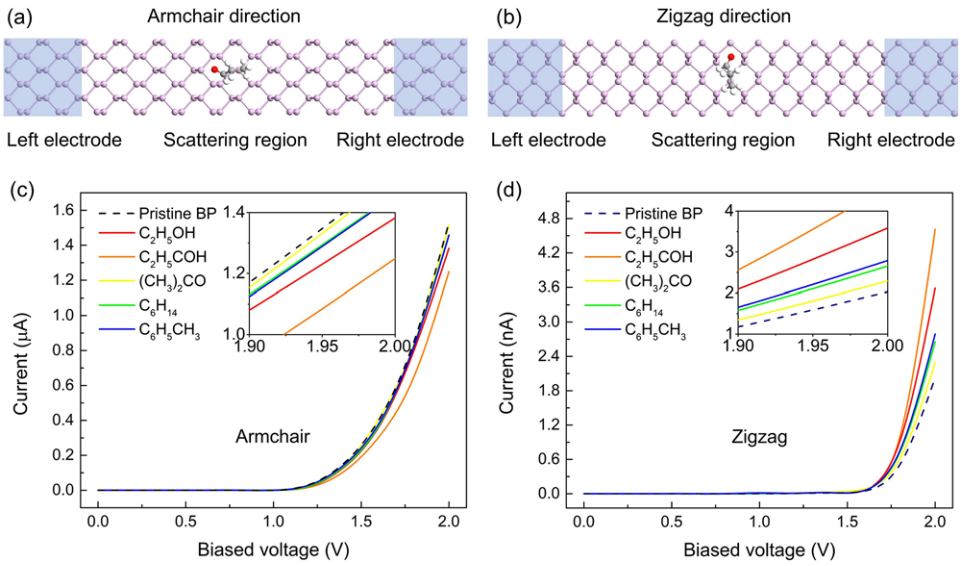

Figure 5. Illustrations of the two-probe systems where semi-infinite left and right electrodes of monolayer BP (blue shaded region) are in contact with the central scattering region with one VOC analyte along a) armchair and b) zigzag direction, respectively. Calculated current–voltage (*I*–*V*) characteristics of monolayer BP before (black dashed line) and after (color solid lines) the exposure of VOCs analytes along c) armchair and d) zigzag direction, respectively.

the pristine monolayer BP exhibits a direct band gap of 0.9 eV, in agreement with previous reported values of 0.91 and 0.80 eV from first-principles studies by Wang et al.[63] and Kulish et al.,[64] respectively, and the experimentally measured transport band gap of 1.0–1.5 eV.[65] We can see that overall the adsorption of VOCs hardly modifies the band gap, exerting rather minor influence on the valence and conduction bands. The adsorbed VOCs molecules only contribute deeply in the valence band within the range from −1.5 to −4.0 eV, producing no noticeable modifications of the DOS near the Fermi level and thus have no relevant influence on the electronic properties. This is consistent with the small adsorption energies of VOCs.

Although the electronic properties of monolayer BP are not much affected by the adsorption of VOCs, the charge transfer induced by the adsorption is expected to affect the resistance of the material system, which can be experimentally measured and serves as a marker for VOCs sensors. To quantitatively estimate the sensitivity of monolayer BP as a VOC sensor, the *I*–*V* characteristics through the material with and without VOC adsorption in the scattering region between two semi-infinite electrodes are studied using the NEGF technique.[50] As shown in **Figure 5**a,b, two semi-infinite electrodes (armchair: 9.14 Å × 9.96 Å, zigzag: 9.96 Å × 9.14 Å) of monolayer BP connect to a central scattering region (armchair: 36.56 Å × 9.96 Å, zigzag: 39.84 Å × 9.14 Å), being built from the preferential VOC adsorption configurations (see Figure 3) previously obtained from DFT calculations. The corresponding *I*–*V* characteristics of monolayer BP with and without VOC adsorption, along the armchair and zigzag directions, are shown in Figure 5c,d, respectively. With a bias voltage applied, the Fermi level of the left electrode shifts upward with respect to that of the right electrode. The current starts to flow only after the valence band maximum (VBM) of the left electrode reaches the conduction band maximum (CBM) of the right electrode. As a result, there is no current passing through the center scattering region when the bias voltage is smaller than ≈0.9 V, the band gap of monolayer BP. As the bias voltage further increases, the currents increase monotonically with the voltage. Comparing Figure 5c and d, we note highly anisotropic *I*–*V* responses along the two directions, with decreased current at the scale of μA along the armchair direction after monolayer BP exposed to VOC analytes, whereas increased current at the scale of nanoAmpere along the zigzag direction. The anisotropic transport properties of monolayer BP originate from its anisotropic electronic band structures, which exhibit much more significant dispersions along the armchair direction, namely the Γ–Y direction in the reciprocal space.[25] Nonetheless, if only the absolute value (in current change) is considered, a similar trend can be observed regardless of the direction, with C_2H_5CHO causing the largest change in current, followed by C_2H_5OH, $C_6H_5CH_3$, C_6H_{14}, and $(CH_3)_2CO$, at a certain applied bias voltage. After the determination of *I*–*V* characteristics of monolayer BP, we further calculate the response of the VOC sensor in terms of the resistance variation. **Figure 6**a presents the normalized response ($\Delta R/R_b$) of the monolayer BP sensor for the five VOCs at bias voltage of 2 V. Here, R_b and ΔR, respectively represent the baseline resistance of the sensor and the change in resistance of the sensor after exposure to VOC analytes. The monolayer BP channel shows similar response behaviors with five VOCs, with the largest increment in resistance of approximately 19% for C_2H_5CHO. The reduction of current or increase of resistance after the VOCs adsorption can be directly measured in experiment.[56]

Besides the sensitivity, another important aspect to assess the performance of a gas sensor is its reusability, which can be typically achieved by heating. Theoretically, the recovery time is predicted by the following equation[66]

$$\tau = \nu^{-1} \exp\left(\frac{|E_{ad}|}{k_B T}\right) \quad (4)$$

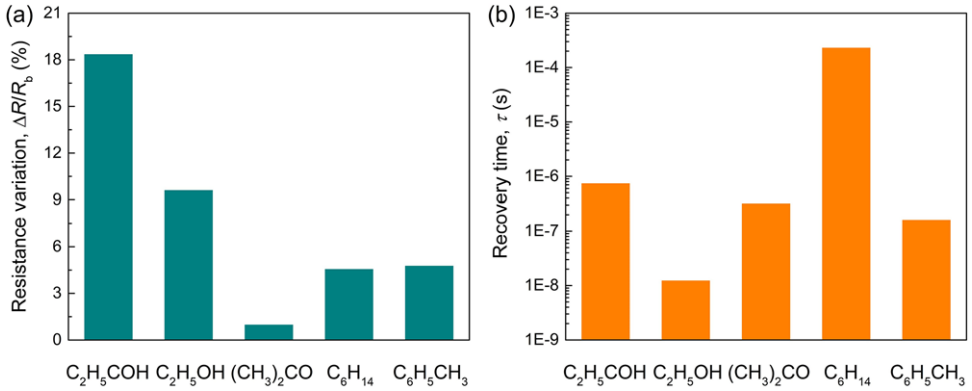

Figure 6. a) The normalized resistance variation under the bias voltage of 2 V, and b) recovery time of the monolayer BP sensor exposed to various VOCs.

where ν denotes the attempt frequency of bond breaking, and thus small $|E_{ad}|$ indicates a fast desorption of VOCs molecules. Calculated from Equation (4), the recovery time (we assume $\nu = 1$ THz and $T = 300$ K) for different VOCs are shown in Figure 6b. We see that C_2H_5CHO, C_2H_6CO, and C_6H_{14} show microsecond scale recovery times while C_2H_6CO exhibits a millisecond scale recovery time. Those τ values are well within the detectable range[31] and indicate very fast recovery.[67–69] One exception is the case of C_2H_5OH, which shows very small recovery time (at 300 K), that is, $\tau = 12.34$ ns, and would be challenging to detect at room temperature. However, microsecond or millisecond scale recovery time may be achieved for C_2H_5OH via strain engineering (to enhance its adsorption energy, as mentioned earlier) or increasing the temperature (e.g., 6.59 μs at 500 K). Therefore, overall, the above demonstrates that monolayer BP promises a good combination of high sensitivity and fast recovery as VOC sensors.

4. Conclusion

In conclusion, we have studied the adsorption of VOCs on monolayer BP using first-principles calculations and examined its potential for application in VOC sensors. The energetically preferable adsorption sites for VOCs on monolayer BP have been identified and the corresponding adsorption energetics have been determined. VOCs were found to generally exhibit stronger interaction with monolayer BP than with the widely studied monolayer MoS_2, indicative of monolayer BP potentially being a more sensitive VOC sensor. The adsorption energetics of VOCs on monolayer BP can be engineered by elastic strain, with compressive (tensile) strain increasing (decreasing) the adsorption energy. Furthermore, the adsorption characteristics of VOCs on monolayer BP are well retained in the event of thickness variation, albeit enhanced adsorption energies for bilayer and few-layer BP. VOC molecules were found to act as charge acceptors and draw charge from monolayer BP, yet have little influence on the electronic properties of monolayer BP. Monolayer BP exhibits highly anisotropic transport properties, nonetheless, the absolute modification of *I*–*V* responses due to VOCs shows a direction-independent trend. Moreover, the recovery time of VOC sensor is found to be within the detectable range and indicative of a short recovery time for next detection. Our findings suggest that monolayer BP can be a compelling candidate material to achieve high sensitivity and good reusability for VOC sensors.

The present study demonstrated the capability of computational modeling as an effective means in the design and exploration of BP-based sensors. However, it is important to recognize that there remain limitations and challenges to be overcome. Taking VOC sensing as an example, realistically there will be coexistence of multiple VOCs. This necessitates the evaluation of the competitive resistance variation and mutual interference between VOCs, and in certain cases, the exact VOC adsorption sequence and possible reconstruction of VOC clusters, in order to obtain a more accurate assessment of VOC sensing and selectivity of BP. Meanwhile, monolayer and multilayer BP can be susceptible to oxygen and water in ambient environment, rendering a serious stability concern for BP-based sensors and making protective functionalization and/or processing treatments a necessity. Consequently, the impact of these treatments on sensing properties and performance of monolayer and multilayer BP needs to be assessed. Moreover, abundant lattice defects and heteroatoms are often expected from the fabrication of BP, which not only may modify the properties of BP but also affect its interaction with VOCs. The above challenges, along with many others not mentioned here, require dedicated research studies and development of new computational tools.

Acknowledgements

This research was supported by the NSERC Discovery grant (grant # RGPIN-2017-05187) and McGill Engineering Doctoral Award (MEDA). The authors also would like to acknowledge the Supercomputer Consortium Laval UQAM McGill and Eastern Quebec for providing computing resources.

Conflict of Interest

The authors declare no conflict of interest.

Keywords

black phosphorus, density functional theory calculations, gas sensors, non-equilibrium Green's function formalism, volatile organic compounds

Received: July 12, 2018
Revised: September 1, 2018
Published online: October 18, 2018

[1] K. S. Novoselov, A. K. Geim, S. V. Morozov, D. Jiang, Y. Zhang, S. V. Dubonos, I. V. Grigorieva, A. A. Firsov, *Science* **2004**, *306*, 666.
[2] H. Liu, A. T. Neal, Z. Zhu, Z. Luo, X. Xu, D. Tománek, P. D. Ye, *ACS Nano* **2014**, *8*, 4033.
[3] M. Buscema, D. J. Groenendijk, G. A. Steele, H. S. J. van der Zant, A. Castellanos-Gomez, *Nat. Commun.* **2014**, *5*, 4651.
[4] M. Engel, M. Steiner, P. Avouris, *Nano Lett.* **2014**, *14*, 6414.
[5] T. Hong, B. Chamlagain, W. Lin, H.-J. Chuang, M. Pan, Z. Zhou, Y.-Q. Xu, *Nanoscale* **2014**, *6*, 8978.
[6] Q. Guo, A. Pospischil, M. Bhuiyan, H. Jiang, H. Tian, D. Farmer, B. Deng, C. Li, S.-J. Han, H. Wang, Q. Xia, T.-P. Ma, T. Mueller,, F. Xia, *Nano Lett.* **2016**, *16*, 4648.
[7] X. Zhang, H. Xie, Z. Liu, C. Tan, Z. Luo, H. Li, J. Lin, L. Sun, W. Chen, Z. Xu, L. Xie, W. Huang, H. Zhang, *Angew. Chem. Int. Ed.* **2015**, *54*, 3653.
[8] D. Li, X. Wang, Q. Zhang, L. Zou, X. Xu, Z. Zhang, *Adv. Funct. Mater.* **2015**, *25*, 7360.
[9] H. Wang, X. Wang, F. Xia, L. Wang, H. Jiang, Q. Xia, M. L. Chin, M. Dubey, S.-j. Han, *Nano Lett.* **2014**, *14*, 6424.
[10] Y. Deng, Z. Luo, N. J. Conrad, H. Liu, Y. Gong, S. Najmaei, P. M. Ajayan, J. Lou, X. Xu, P. D. Ye, *ACS Nano* **2014**, *8*, 8292.
[11] P. Gehring, R. Urcuyo, D. L. Duong, M. Burghard, K. Kern, *Appl. Phys. Lett.* **2015**, *106*, 233110.
[12] J. Miao, S. Zhang, L. Cai, C. Wang, *Adv. Electron. Mater.* **2016**, *2*, 1500346.
[13] P. J. Jeon, Y. T. Lee, J. Y. Lim, J. S. Kim, D. K. Hwang, S. Im, *Nano Lett.* **2016**, *16*, 1293.
[14] L. Chen, G. Zhou, Z. Liu, X. Ma, J. Chen, Z. Zhang, X. Ma, F. Li, H.-M. Cheng, W. Ren, *Adv. Mater.* **2016**, *28*, 510.
[15] C. Hao, B. Yang, F. Wen, J. Xiang, L. Li, W. Wang, Z. Zeng, B. Xu, Z. Zhao, Z. Liu, Y. Tian, *Adv. Mater.* **2016**, *28*, 3194.
[16] L. Shulenburger, A. D. Baczewski, Z. Zhu, J. Guan, D. Tomanek, *Nano Lett.* **2015**, *15*, 8170.
[17] L. Li, Y. Yu, G. J. Ye, Q. Ge, X. Ou, H. Wu, D. Feng, X. H. Chen, Y. Zhang, *Nat. Nanotechnol.* **2014**, *9*, 372.
[18] L. Liang, J. Wang, W. Lin, B. G. Sumpter, V. Meunier, M. Pan, *Nano Lett.* **2014**, *14*, 6400.
[19] H. Liu, Y. Du, Y. Deng, D. Y. Peide, *Chem. Soc. Rev.* **2015**, *44*, 2732.
[20] R. Hultgren, N. Gingrich, B. Warren, *J. Chem. Phys.* **1935**, *3*, 351.
[21] H. Liu, A. T. Neal, Z. Zhu, X. Xu, D. Tomanek, P. D. Ye, Z. Luo, *ACS Nano* **2014**, *8*, 4033.
[22] P. Yasaei, B. Kumar, T. Foroozan, C. Wang, M. Asadi, D. Tuschel, J. E. Indacochea, R. F. Klie, A. Salehi-Khojin, *Adv. Mater.* **2015**, *27*, 1887.
[23] J. R. Brent, N. Savjani, E. A. Lewis, S. J. Haigh, D. J. Lewis, P. O'Brien, *Chem. Commun.* **2014**, *50*, 13338.
[24] W. Lu, H. Nan, J. Hong, Y. Chen, C. Zhu, Z. Liang, X. Ma, Z. Ni, C. Jin, Z. Zhang, *Nano Res.* **2014**, *7*, 853.
[25] L. Kou, T. Frauenheim, C. Chen, *J. Phys. Chem. Lett.* **2014**, *5*, 2675.
[26] N. Suvansinpan, F. Hussain, G. Zhang, C. H. Chiu, Y. Cai, Y.-W. Zhang, *Nanotechnology* **2016**, *27*, 065708.
[27] A. N. Abbas, B. Liu, L. Chen, Y. Ma, S. Cong, N. Aroonyadet, M. Köpf, T. Nilges, C. Zhou, *ACS Nano* **2015**, *9*, 5618.
[28] Q. He, Z. Zeng, Z. Yin, H. Li, S. Wu, X. Huang, H. Zhang, *Small* **2012**, *8*, 2994.
[29] D. J. Late, Y.-K. Huang, B. Liu, J. Acharya, S. N. Shirodkar, J. Luo, A. Yan, D. Charles, U. V. Waghmare, V. P. Dravid, *ACS Nano* **2013**, *7*, 4879.
[30] S. Cui, H. Pu, S. A. Wells, Z. Wen, S. Mao, J. Chang, M. C. Hersam, J. Chen, *Nat. Commun.* **2015**, *6*, 8632.
[31] S.-Y. Cho, Y. Lee, H.-J. Koh, H. Jung, J.-S. Kim, H.-W. Yoo, J. Kim, H.-T. Jung, *Adv. Mater.* **2016**, *28*, 7020.
[32] C. C. Mayorga-Martinez, Z. Sofer, M. Pumera, *Angew. Chem. Int. Ed.* **2015**, *54*, 14317.
[33] G. Lee, S. Jung, S. Jang, J. Kim, *Appl. Phys. Lett.* **2017**, *110*, 242103.
[34] S.-Y. Cho, H.-J. Koh, H.-W. Yoo, H.-T. Jung, *Chem. Mater.* **2017**, *29*, 7197.
[35] S. K. Arya, S. Bhansali, *Chem. Rev.* **2011**, *111*, 6783.
[36] M. Hakim, Y. Y. Broza, O. Barash, N. Peled, M. Phillips, A. Amann, H. Haick, *Chem. Rev.* **2012**, *112*, 5949.
[37] B. Buszewski, A. Ulanowska, T. Ligor, N. Denderz, A. Amann, *Biomed. Chromatogr.* **2009**, *23*, 551.
[38] C. Turner, P. Španěl, D. Smith, *Rapid Commun. Mass Spectrom.* **2006**, *20*, 61.
[39] J. W. Grate, S. L. Rose-Pehrsson, D. L. Venezky, M. Klusty, H. Wohltjen, *Anal. Chem.* **1993**, *65*, 1868.
[40] C. Di Natale, A. Macagnano, E. Martinelli, R. Paolesse, G. D'Arcangelo, C. Roscioni, A. Finazzi-Agrò, A. D'Amico, *Biosens. Bioelectron.* **2003**, *18*, 1209.
[41] S. J. Ray, M. V. Kamalakar, R. Chowdhury, *J. Phys. Condens. Matter* **2016**, *28*, 195302.
[42] G. Kresse, D. Joubert, *Phys. Rev. B* **1999**, *59*, 1758.
[43] J. P. Perdew, K. Burke, M. Ernzerhof, *Phys. Rev. Lett.* **1996**, *77*, 3865.
[44] S. Grimme, J. Antony, S. Ehrlich, H. Krieg, *J. Chem. Phys.* **2010**, *132*, 154104.
[45] Y. Cai, G. Zhang, Y.-W. Zhang, *Sci. Rep.* **2014**, *4*, 6677.
[46] J. Qiao, X. Kong, Z.-X. Hu, F. Yang, W. Ji, *Nat. Commun.* **2014**, *5*, 4475.
[47] T. Hu, J. Hong, *J. Phys. Chem. C* **2015**, *119*, 8199.
[48] B. Li, P. Ou, Y. Wei, X. Zhang, J. Song, *Materials* **2018**, *11*, 726.
[49] B. Ouyang, J. Song, *Appl. Phys. Lett.* **2013**, *103*, 102401.
[50] M. Br,byge, J.-L. Mozos, P. Ordejón, J. Taylor, K. Stokbro, *Phys. Rev. B* **2002**, *65*, 165401.
[51] Y. Xue, S. Datta, S. Hong, R. Reifenberger, J. I. Henderson, C. P. Kubiak, *Phys. Rev. B* **1999**, *59*, R7852.
[52] Q. H. Wang, K. Kalantar-Zadeh, A. Kis, J. N. Coleman, M. S. Strano, *Nat. Nanotechnol.* **2012**, *7*, 699.
[53] S. Lebègue, T. Björkman, M. Klintenberg, R. M. Nieminen, O. Eriksson, *Phys. Rev. X* **2013**, *3*, 031002.
[54] X.-Q. Tian, L. Liu, X.-R. Wang, Y.-D. Wei, J. Gu, Y. Du, B. I. Yakobson, *J. Mater. Chem. C* **2017**, *5*, 1463.
[55] H. Pu, S. Rhim, M. Gajdardziksa-Josifovska, C. Hirschmugl, M. Weinert, J. Chen, *RSC Adv.* **2014**, *4*, 47481.
[56] J.-S. Kim, H.-W. Yoo, H. O. Choi, H.-T. Jung, *Nano Lett.* **2014**, *14*, 5941.
[57] Q. Wei, X. Peng, *Appl. Phys. Lett.* **2014**, *104*, 251915.
[58] B. Sa, Y.-L. Li, J. Qi, R. Ahuja, Z. Sun, *J. Phys. Chem. C* **2014**, *118*, 26560.
[59] G. Henkelman, A. Arnaldsson, H. Jónsson, *Comput. Mater. Sci.* **2006**, *36*, 354.
[60] E. Sanville, S. D. Kenny, R. Smith, G. Henkelman, *J. Comput. Chem.* **2007**, *28*, 899.
[61] W. Tang, E. Sanville, G. Henkelman, *J. Phys. Condens. Matter* **2009**, *21*, 084204.
[62] M. Yu, D. R. Trinkle, *J. Chem. Phys.* **2011**, *134*, 064111.
[63] C. Wang, Q. Xia, Y. Nie, G. Guo, *J. Appl. Phys.* **2015**, *117*, 124302.
[64] V. V. Kulish, O. I. Malyi, C. Persson, P. Wu, *Phys. Chem. Chem. Phys.* **2015**, *17*, 992.

[65] H. O. H. Churchill, P. Jarillo-Herrero, *Nat. Nanotechnol.* **2014**, *9*, 330.
[66] V. Babar, S. Sharma, U. Schwingenschlögl, *Adv. Theory Simul.* **2018**, *1*, 1700008.
[67] J. Kong, N. R. Franklin, C. Zhou, M. G. Chapline, S. Peng, K. Cho, H. Dai, *Science* **2000**, *287*, 622.
[68] S.-Y. Cho, H.-W. Yoo, J. Y. Kim, W.-B. Jung, M. L. Jin, J.-S. Kim, H.-J. Jeon, H.-T. Jung, *Nano Lett.* **2016**, *16*, 4508.
[69] D. Liu, X. Lian, A. K. Mallik, W. Han, F. Wei, J. Yuan, C. Yu, G. Farrell, Y. Semenova, Q. Wu, presented at 25th Int. Conf. on Opt. Fiber Sens., Jeju, Korea, April 2017.